

# Photorealistic Reproduction with Anisotropic Reflection on Mobile Devices using Densely Sampled Images

Shoichiro Mihara, Haruhisa Kato and Masaru Sugano

*KDDI Research, Inc., Saitama, Japan*

**Keywords:** Photorealistic Reproduction, Augmented Reality, Image-based Rendering.

**Abstract:** Photorealistic reproduction of real objects with complexities of geometry and optics on mobile devices has been a long-standing challenge in augmented reality owing to the difficulties of modeling and rendering the real object faithfully. Although image-based rendering, which does not require the objects to be modeled, has been proposed, it still fails to photorealistically reproduce the object's complete appearance containing complex optical properties such as anisotropic reflection. We propose a novel system for use on mobile devices capable of reproducing real objects photorealistically from all angles based on new view generation using densely sampled images. In order to realize the proposed system, we developed a method of selecting the image closest to a given camera view from densely sampled images by quantifying the similarity of two rays, performed rigid geometric transformation to preserve the vertical direction for stable viewing, and introduced color correction for consistency of color between the generated view and the real world. Through experiments, we confirmed that our proposed system can reproduce real objects with complex optical properties more photorealistically compared with conventional augmented reality.

## 1 INTRODUCTION

Applications designed to reproduce real objects have become widespread throughout the market, especially applications for mobile devices. For example, in electronic commerce, applications for mobile devices such as *IKEA Place*<sup>1</sup> are available that make it possible for the appearance of items to be observed as if they were at hand by rendering them overlaid on a real-world background; this is based on a technique called augmented reality. However, the appearance of the objects reproduced by these applications is not photorealistic because they are not rendered based on materials faithful to the original objects.

Modern rendering techniques can be classified into two different categories; model-based rendering and image-based rendering (Levoy and Hanrahan, 1996)(Gortler et al., 1996). As for model-based rendering, the reflectance properties represented by a bidirectional reflectance distribution function (BRDF) is necessary to render objects photorealistically. However, to measure anisotropic BRDF which arises from microstructures such as a hairline processed metal or woven fabric, an expensive measuring instrument and an enormous amount of measuring time are required due to the need to observe

light reflected at the object surface in all directions. Image-based rendering that does not rely on geometric representation has been proposed to reproduce real objects or scenes by synthesizing virtual views from arbitrary camera positions using densely sampled images from a real or virtual environment. Although it is a technique powerful enough to reproduce high-quality virtual views, it still fails to photorealistically reproduce the complete appearance containing complex optical properties such as anisotropic reflection because it is essentially based on interpolation of discretely sampled images which can miss capturing pronounced variations in anisotropic reflection, which is highly sensitive to viewing direction.

In this research, we propose a novel system for use on mobile devices that can reproduce real objects photorealistically by generating new views from all angles using densely sampled images. Our proposed system can be utilized for various applications: for example, examining unique cultural assets or rare minerals for educational purposes, viewing items sold on online shopping sites, and enjoying a realistic virtual world for entertainment. The proposed system has three main advantages. First, as with image-based rendering, it can reproduce objects photorealistically without constructing a geometric representation. Second, our proposed system can be easily implemented and run on mobile devices with meager

<sup>1</sup><http://www.ikea.com/gb/en/customer-service/ikea-apps/>



Figure 1: Problem of defining the similarity of camera poses equivalent to rays. Which one is closer to each other?

computational resources, because it depends on simple manipulation of 2D-images. Third, the direction of generated view is not limited to object-centered direction, whereas image-based rendering implicitly assumes that the camera always faces objects. That is owing to our proposed method of quantifying the similarity of the position and orientation of the cameras (referred to as camera poses). It is problematic to define the similarity of camera poses due to differences in unit and range, which is equivalent to defining the similarity of two rays as shown in Fig. 1. Because this problem has not been sufficiently studied to date, we address it in this research.

In order to realize the proposed system, we suggest several methods described in following contributions and introduce the color correction method for consistency of color between the generated view and the real world. Our major technical contributions are:

1. We propose a novel system to be run on mobile devices that has been designed to reproduce objects photorealistically from all angles. (Section 3)
2. We propose a unique method of selecting the image closest to a given camera view from densely sampled images by quantifying the similarity of two rays. (Section 3.1)
3. We propose a well-designed rigid geometric transformation preserving the vertical direction for stable viewing. This is achieved by performing translation, rotation, and scaling sequentially. (Section 3.2)

This paper explains the proposed methods and shows how the proposed system improves the reality of the displayed objects by conducting experiments in which we compare the results of the proposed system with conventional augmented reality.

## 2 RELATED WORK

The simplest way to measure the BRDF is using a gonioreflectometer (Nicodemus et al., 1977). But a vast amount of measurement time is required since the BRDF is measured with all combinations of the incident and reflection directions by moving the light source and the sensors. Therefore, studies on how to improve BRDF measurement efficiency have been conducted (Mukaigawa et al., 2009)(Tunwattanapong

et al., 2013)(Ward et al., 2014). Although it becomes possible to measure BRDF that is not spatially uniform in a 3D shape within a relatively short time, there are still the limitations, for example, the inability to measure translucent objects and objects with concave surfaces.

An image-based rendering technique relies on densely sampled images and can be classified into two fundamentally different approaches. The first approach is based on the concept of *light field* (Levoy and Hanrahan, 1996)(Gortler et al., 1996). It represents the light ray as a 4D function of position and direction, constructed with densely sampled images. Virtual views from arbitrary camera positions can be synthesized by extracting slices from the light field and interpolating rays in an appropriate way. The second approach is based on estimating the approximate geometry in the form of depth maps (Shade et al., 1998)(Sinha et al., 2012). Some sampled images are chosen based on the virtual camera position, warped using the depth maps, and combined for new view synthesis. An important advantage of these approaches is that they can synthesize photorealistic virtual views with no or very little geometry information and no explicit representation of optical properties of the objects. However, if their techniques are applied to the reproduction of complex optical properties which vary considerably depending on the viewing angle, such as anisotropic reflection, undesirable artifacts of blurring and edge ghosting will occur. This is because image-based rendering is essentially based on interpolation of discretely sampled images, even though some variants have been proposed to increase realism of the rendered views (Wood et al., 2000)(Shum et al., 2004)(Vagharshakyan et al., 2015). Consequently, as we assume that target objects have some complex optical properties as mentioned above, we purposely do not depend on interpolation techniques derived from image-based rendering. Instead we propose simple manipulation of 2D-images which can produce acceptable results for our assumed applications described in Section 5.

Photo-based augmented reality which reproduces objects using densely sampled images has been proposed by Ohta et al. (Ohta et al., 2012). This approach is based on a kind of view-dependent texture mapping (Debevec et al., 1996). It has the same advantage as image-based rendering which is able to reproduce objects efficiently and photorealistically without a 3D model. In addition, they proposed adding a method to correct the difference in color tone between the sampled images and the real environment (Ohta et al., 2013). However, there is a problem that the reproduced objects appear to be unnatural as they do with

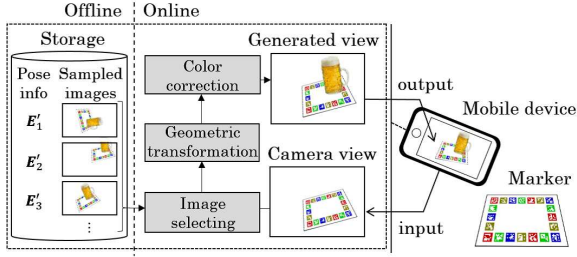


Figure 2: Conceptual diagram of the proposed system.

conventional augmented reality because only the object image is superimposed on the background of the real environment and global illumination effects like shadowing and interreflection between the object and the surroundings cannot be reproduced.

Meanwhile, Suzuki et al. proposed a substitutional reality that convinces the user that he/she is perceiving a live reality instead of another reality (or past reality) by showing the user a movie taken in the past without the user noticing a reality gap (Suzuki et al., 2012). By switching between the real-world video obtained from the camera mounted on the HMD worn by the user and the video recorded at the same place in the past alternately without the user being aware of it, there arises a state in which the user mistakenly perceives the recorded video as the real world. The limitation of their system is that the user’s viewpoint must be fixed at the place where the video was recorded. Although their research aimed at psychologically verifying the concept of substitutional reality, it is also applicable to augmented reality in that it employs a phenomenon whereby past images are perceived as the live reality, and our proposed system is inspired by substitutional reality.

We propose a novel system so that the reproduced objects are perceived as if they exist in front of the eyes, and which performs object reproduction by substituting the image generated with densely sampled images without estimating the explicit geometry of the scene and BRDF of the target object.

### 3 PROPOSED SYSTEM

A conceptual diagram of the proposed system is shown in Fig. 2. In an offline process, a collection of images is sampled from all angles so that the object to be reproduced (hereinafter referred to as the target object) and the marker within the angle of view are saved in the storage space along with the pose information, which is described in the next section. In the online process, the user holds the mobile device in front of his/her face, shoots the marker with the

camera mounted on the device, and views the image displayed on the screen from various angles. First, the camera pose relative to the world coordinate system is estimated based on the marker designed as described in Section 3.3, the similarities of the pose information between of the camera view and of every sampled image are evaluated, and the sampled image corresponding to the most similar pose is selected. Then, the selected image undergoes rigid geometric transformation so that it can be seen from the camera pose. In the color correction process, the difference in color tone between the sampled images and the camera view is corrected, and the processed image is displayed on the screen of the device. Details of each process are described below.

#### 3.1 Image Selection by Quantifying a Similarity of Camera Poses

In this section, we explain how to select the sampled image based on the similarity of the camera pose. Conventional image-based rendering assumes that possible views face the object center and sampled images are selected based on only the distance between viewpoints, ignoring the direction of view. However, our system is designed to be used on mobile devices where the viewpoints and directions can be easily changed. Therefore, our proposed method should be able to select a correct image from the sample collection that matches the given camera pose including the direction of view.

Coordinate transformations between the world coordinate  $(X, Y, Z)$  and the camera coordinate  $(x, y, z)$  are denoted as

$$[x y z]^T = \mathbf{R}[X Y Z]^T + \mathbf{t}, \quad (1)$$

where  $\mathbf{t}$  is the translation vector and  $\mathbf{R}$  is the rotation matrix (Tsai, 1987). If we evaluate the similarity of the camera poses as the collective difference of  $\mathbf{t}$ s and  $\mathbf{R}$ s, it is necessary to perform weighting to correct the gap between the unit and range of these parameters. However, appropriate weight depends on the scale of  $\mathbf{t}$  which can change during operation. Therefore, we propose a method to quantify the similarity of camera poses by expressing them as a six-dimensional quantity representing the camera view ray.

First, the position of the target object in the world coordinate system is defined as the target point  $P_{\text{tar}}(X_t, Y_t, Z_t)$  by the user. Then, the foot of the perpendicular from the target point  $P_{\text{tar}}$  to the visual line extending from the camera viewpoint  $P_{\text{cam}}(X_c, Y_c, Z_c)$  is defined as the gaze point  $P_{\text{gaz}}(X_g, Y_g, Z_g)$  as shown in Fig. 3(a). When the translational vector  $\mathbf{t}$  and rotation matrix  $\mathbf{R}$  of the camera are estimated, the coor-

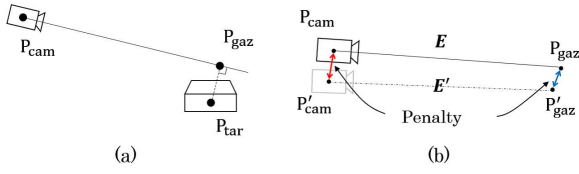


Figure 3: Conceptual diagram to explain how to define the similarity of camera poses: (a) definition of object point and gaze point; (b) penalty definition for evaluating similarity of camera poses.

Coordinates of viewpoint  $P_{cam}$  and gaze point  $P_{gaz}$  can be obtained from the following equations.

$$[X_c Y_c Z_c]^T = -R^T t, \quad (2)$$

$$[X_g Y_g Z_g]^T = [X_c Y_c Z_c]^T + e^T R [X_{tc} Y_{tc} Z_{tc}]^T R^T e, \quad (3)$$

where  $[X_{tc} Y_{tc} Z_{tc}]^T = [X_c - X_t Y_c - Y_t Z_c - Z_t]^T$  and  $e$  is a unit vector of the visual line on the camera coordinate system. Finally, the camera pose can be represented by combining  $(X_c, Y_c, Z_c)$  and  $(X_g, Y_g, Z_g)$  into a six-dimensional quantity, defined as visual line segment  $E$ :

$$E \equiv (X_c, Y_c, Z_c, X_g, Y_g, Z_g). \quad (4)$$

The penalty of camera pose similarity is quantified by the Euclidean distance between  $E$ , which represents certain camera pose, and  $E'$ , which represents another pose, as shown in Fig. 3(b). In the proposed system, sampled images and visual line segments  $E'_i$  are stored in a storage space ( $i$  is an index of stored images), and the index  $i_{\min}(t)$  of the visual line segment which most closely resembles the visual line segment of the user camera  $E(t)$  is calculated at each time  $t$  by

$$i_{\min}(t) = \arg \min_i \|E(t) - E'_i\|_2. \quad (5)$$

When the penalty is small, the viewpoint and the direction of the visual line approach one another and the overlapping of the imaging ranges of the cameras becomes larger. The remaining gap between views corresponding to  $E(t)$  and  $E'_{i_{\min}(t)}$  is corrected by geometric transformation described in the next section.

### 3.2 Generation of Displayed Image by Geometric Transformation

Because the sampled images are captured from discrete camera poses, translation and orientation of the image (referred to as image pose) selected by equation (5) may be different from the image pose of the camera. In order to generate the new view, rigid geometric transformation is performed on the selected

image to correct the difference of image pose. In this section, we propose a method of sequential similarity transformation that can convert the image pose in more stable condition while maintaining the object shape.

#### 3.2.1 Homography Transformation

As a naive method, homography transformation can be performed to match the marker planes in the selected image and the camera image to match their image pose. However, when homography transformation between the planes is performed, the shape of the three-dimensional object is deformed. This is not acceptable for the proposed system.

#### 3.2.2 Similarity Transformation

To generate displayed images while maintaining the object shape, similarity transformation can be used as a naive method. Similarity transformations between the image coordinates  $(x, y)$  and  $(x', y')$  are denoted by the following equation.

$$\begin{bmatrix} x \\ y \\ 1 \end{bmatrix} = \begin{bmatrix} s \cos \theta & -s \sin \theta & t_x \\ s \sin \theta & s \cos \theta & t_y \end{bmatrix} \begin{bmatrix} x' \\ y' \\ 1 \end{bmatrix}, \quad (6)$$

where  $\theta$  is the rotation angle,  $[t_x t_y]^T$  is the translation vector and  $s$  is the scale transformation in the image plane. By using coordinates of corresponding points based on the marker within the sampled image and the camera view, the similarity transformation matrix is estimated by the least squares method. However, when the camera pose changes over time, all parameters of the matrix may fluctuate due to the estimation error. Therefore, the view generated by similarity transformation may make the image pose unstable, giving the user an unnatural impression. This problem can be solved by sequential similarity transformation as described below.

#### 3.2.3 Sequential Similarity Transformation

Because the generated view of the proposed system is viewed as if it is captured by the device's camera, the scale value  $s$  cannot be distinguished from the zoom operation. To make the best use of this feature, we propose a method of sequential similarity transformation to stabilize the image pose of the generated view by removing the error fluctuation from the rotation angle  $\theta$  and the translation vector  $[t_x t_y]^T$  and allowing the error only on the scale value  $s$ , which can be temporally smoothed.

First, the world landmark vector  $u_{wld}$  is defined as shown in Fig. 4 (how to define it is described at

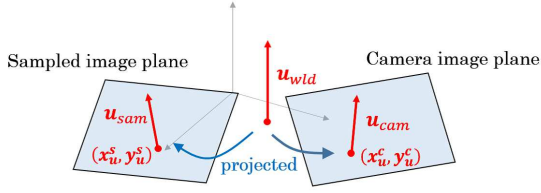


Figure 4: Conceptual diagram of world landmark vector and projection to image planes (Note that the image planes are actually closer).

the end of this section). Then, the vector  $\mathbf{u}_{wld}$  is projected to the camera image plane and the sampled image plane, and let the projected vectors be  $\mathbf{u}_{cam}$  and  $\mathbf{u}_{sam}$  respectively. The vector from the initial point  $(x_u^s, y_u^s)$  of  $\mathbf{u}_{sam}$  to the initial point  $(x_u^c, y_u^c)$  of  $\mathbf{u}_{cam}$  is defined as translation vector  $\mathbf{t}_u$  and the angle  $\theta_u$  between  $\mathbf{u}_{cam}$  and  $\mathbf{u}_{sam}$  are calculated:

$$\mathbf{t}_u = [x_u^c \ y_u^c]^T - [x_u^s \ y_u^s]^T, \quad (7)$$

$$\theta_u = \text{sgn}(\mathbf{u}_{sam} \times \mathbf{u}_{cam}) \arccos\left(\frac{\mathbf{u}_{sam} \cdot \mathbf{u}_{cam}}{|\mathbf{u}_{sam}| |\mathbf{u}_{cam}|}\right), \quad (8)$$

where the counterclockwise direction is positive.

Second, the sampled image is transformed sequentially with the translation vector  $\mathbf{t}_u$ , then rotation is performed with the angle  $\theta_u$  around the initial point  $(x_u^c, y_u^c)$  of  $\mathbf{u}_{cam}$ . Rotation matrix  $\mathbf{R}_u$  is obtained by

$$\mathbf{R}_u = \begin{bmatrix} \cos \theta_u & -\sin \theta_u & x_u^c(1 - \cos \theta_u) + y_u^c \sin \theta_u \\ \sin \theta_u & \cos \theta_u & -x_u^c \sin \theta_u + y_u^c(1 - \cos \theta_u) \end{bmatrix}. \quad (9)$$

The scale value  $s_u$  is estimated by the least squares method, which matches the scale of the sampled image to the camera view. Denoting the coordinates of the corresponding point group based on the marker within the camera image and the sampled image as  $(x_j^c, y_j^c)$  and  $(x_j^s, y_j^s)$  respectively, the scale value fitting  $(x_j^c, y_j^c)$  and the point group obtained by translating and rotating  $(x_j^s, y_j^s)$  using  $\mathbf{t}_u$  and  $\mathbf{R}_u$  is expressed by the following equation

$$\begin{bmatrix} x_j^c - x_u^c \\ y_j^c - y_u^c \end{bmatrix} = s_u \left\{ \mathbf{R}_u \left( \begin{bmatrix} x_j^s \\ y_j^s \\ 1 \end{bmatrix} \right) + \begin{bmatrix} \mathbf{t}_u \\ 0 \end{bmatrix} \right\} - \begin{bmatrix} x_u^c \\ y_u^c \end{bmatrix}. \quad (10)$$

Let  $\mathbf{b}_c$  and  $\mathbf{A}_s$  be the matrices composed of the vertical vectors of the left and right side of equation (10) of all the corresponding points respectively, the scale value  $s_u$  is calculated by the least squares method as

$$s_u = (\mathbf{A}_s^T \mathbf{A}_s)^{-1} \mathbf{A}_s^T \mathbf{b}_c. \quad (11)$$

As mentioned above, the magnitude of the error of  $s_u$  cannot be distinguished from the zoom operation.

Hence, when the system runs over time, it is reasonable to smooth  $s_u(t)$  with parameter  $M$  to suppress the fluctuation of the scale of the displayed image by calculating

$$\bar{s}_u(t) = \frac{1}{M+1} \sum_{k=t-M}^t s_u(k). \quad (12)$$

Finally, the new view is generated by translating, rotating, and scaling the selected sampled image sequentially with  $\mathbf{t}_u$ ,  $\mathbf{R}_u$  and  $\bar{s}_u$ . Additionally, we can clip an appropriately sized central area from the generated view since there is an unmapped area at the edge of it.

Next, how to define the world landmark vector  $\mathbf{u}_{wld}$  is described below. Although  $\mathbf{u}_{wld}$  can be defined as an arbitrary vector, a vector within the imaging range of the camera image and the sampled image is appropriate because sequential similarity transformation is based on the position and orientation of  $\mathbf{u}_{wld}$  projected onto both images. Furthermore, since the proposed system assumes the target object is stationary, the object should seem to be stationary, or standing upright. Because humans perceive something as upright if it is consistent with the direction of gravity (Rock, 1974), it is expected that the object would appear to be upright if the direction of gravity in the generated view is aligned with the direction in the camera view that is the actual direction of gravity. Therefore, we define  $\mathbf{u}_{wld}$  as a vector parallel to the direction of gravity, where the initial point is camera's gaze point  $P_{gaz}$ .

### 3.3 Correction of Color Tone

Our proposed system generates new views entirely from densely sampled images. Consequently, if the illumination environment is different from that when the sampled images were captured, the color tone of the sampled images may appear unnatural. In order to make the color tone of the generated views compatible with the actual illumination, we introduce the color correction method proposed by Reinhard et al. (Reinhard et al., 2001). They matched the color tone between images not by estimating ambient light but by adjusting the statistical values (average and standard deviation) of each color channel after converting RGB color into  $\alpha\beta$  color space (Ruderman et al., 1998) that has a low correlation with each channel. Although colors under actual illumination are not completely reproduced, we can take advantage of the simplicity and effectiveness of their method.

In order to introduce the color correction method into the proposed system, we use a colored marker board as shown in Fig. 5. The marker group is generated by ArUco (Garrido-Jurado et al., 2014) and each

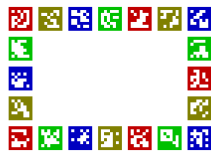


Figure 5: Colored marker board of the proposed system.

marker is painted arbitrarily with one of the RGB colors of red(192, 0, 0), green(0, 192, 0), blue(0, 0, 192), or yellow(128, 128, 0). Considering that the  $\alpha$  and  $\beta$  channels correspond to the complementary color axes of yellow-blue and red-green respectively, the marker's colors are adjusted to ensure that the standard deviation of each channel is not too small and is detectable by ArUco. The proposed system assumes that the user looks at the generated view while capturing the marker board of Fig. 5 and at least part of the marker is within the angle of view of every sampled image. Therefore, some of the same markers of the colored marker board can be detected and identified by ArUco in the selected image and the camera image. Then, by matching the statistical values of  $l\alpha\beta$  channels obtained from the pixel values in the color reference area that is the internal area of the markers identified in both the sampled image and the camera image, it is possible to make the color tone of the generated view compatible with the actual illumination environment.

Although we use the square fiducial marker in this paper, we can also use any 2D images which have features detectable with any well-known keypoint detector and descriptor (Rublee et al., 2011)(Alcantarilla et al., 2013) as long as the color distribution of the image is not too small such as that of a black-and-white image. By dividing the image into several identifiable areas corresponding to each of the markers, we can perform color correction in the same manner as described above.

## 4 EXPERIMENTS

Using computer graphics simulation and a prototype system, we conducted several experiments to validate the effectiveness of the proposed system. We compared the shape of the object in the virtual views generated by naive transformation and sequential similarity transformation using computer graphics (Section 4.1). Color correction is verified by application to real images having several color tones (Section 4.2). We then demonstrate that the proposed system can reproduce the objects with anisotropic reflection or microstructures (Section 4.3). We conducted a subjective experiment to validate the capability of the pro-

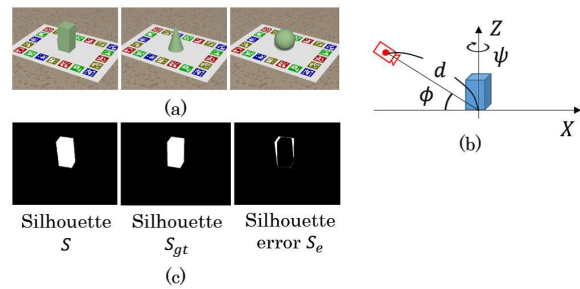


Figure 6: Settings of evaluation experiment of sequential similarity transformation: (a) example of sampled images; (b) camera settings for generating the sampled images using computer graphics; (c) example of silhouette  $S$ ,  $S_{gt}$  and silhouette error  $S_e$  visualized as a binary image.

posed system to reproduce objects naturally and photorealistically compared to conventional augmented reality.

### 4.1 Evaluation of Sequential Similarity Transformation

In order to verify how the shape of objects is displayed by sequential similarity transformation compared with the other naive transformations, we conducted the simulation experiment using computer graphics. The sampled images are generated using *POV-Ray*<sup>2</sup>, in which a solid primitive object, i.e., a cuboid, cone, or sphere, is put on the colored marker board and rendered with the camera settings as shown in Fig. 6(a)(b). The gaze point is fixed at the center of the marker board, distance to the gaze point is fixed at  $d$  ( $= 6.0$  in our experiment), the depression angle  $\phi$  is fixed at  $30^\circ$  (actually, we incremented  $\phi$  by  $10^\circ$  from  $20^\circ$  to  $70^\circ$ , but no different trend was found in the results so we mention only  $30^\circ$  for the sake of simplicity), and the azimuth angle  $\psi$  is incremented by  $10^\circ$ . Then, 360 camera images are generated by rendering only the marker board with the same camera settings except for the azimuth angle  $\psi$  that is incremented by  $1^\circ$ . The ground truth images are generated by rendering the primitive object onto each camera image. Using the sampled images and the camera images, the virtual views are generated by the proposed system based on homography transformation, similarity transformation, and sequential similarity transformation (hereinafter referred to as Hom-trans., Sim-trans., and Proposed-trans., respectively). To compare the generated views between each transformation, the silhouette  $S$  of the object is extracted. Then, we define the difference between  $S$  and the silhouette  $S_{gt}$  extracted from the ground truth image as the silhouette error  $S_e = S \cup S_{gt} - S \cap S_{gt}$ , and  $n(S_e)$  is

<sup>2</sup><http://www.povray.org/>

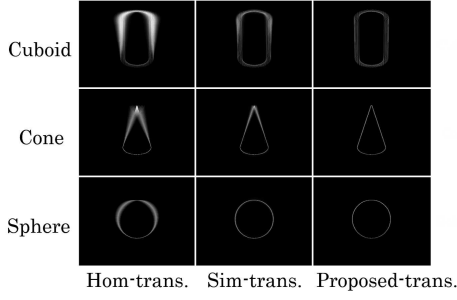


Figure 7: Comparison of the distribution of silhouette error among Hom-trans., Sim-trans., and Proposed-trans.

Table 1: Average of  $n(S_e)$  calculated from all views generated by Hom-trans., Sim-trans., and Proposed-trans. The unit is pixel.

	Cuboid	Cone	Sphere
Hom-trans.	2245.29	1471.35	1208.39
Sim-trans.	839.61	672.49	473.44
Proposed-trans.	521.71	317.58	290.59

calculated as an evaluation value that is the number of pixels in  $S_e$ . Fig. 6(c) shows an example of silhouette  $S$  and  $S_{gt}$ , and silhouette error  $S_e$ .

We generated the views by Hom-trans., Sim-trans., and Proposed-trans. for all camera images and calculated silhouette errors  $S_e$ , and evaluated the results with the average of  $n(S_e)$  as shown in Table 1. It can be seen that  $n(S_e)$  of Proposed-trans. is smaller than the other transformations. Additionally, Fig. 7 shows the distribution of the silhouette error  $S_e$  visualized by summing up  $S_e$  assumed as binary images and normalized to a range of  $[0, 255]$ . We can see that the distribution of Proposed-trans. is narrower than the other transformations. From the above results, we confirmed that by using Proposed-trans., the displayed shape of an object was closest to the ground truth and the position and orientation of the object were maintained more stably compared with the other transformations.

## 4.2 Evaluation of Color Correction

To verify how the color tones of the sampled images are converted by the color correction described in Section 3.3, we conducted an experiment using real images.

The colored marker board was printed on plain paper and captured with the car model using a Logicool web camera (C920) under a fluorescent lamp, setting the white balance (WB) for a color temperature of 4000K. The captured image is used as the sampled image as shown in Fig. 8 (middle-left). The images captured from the same camera position with WB ad-

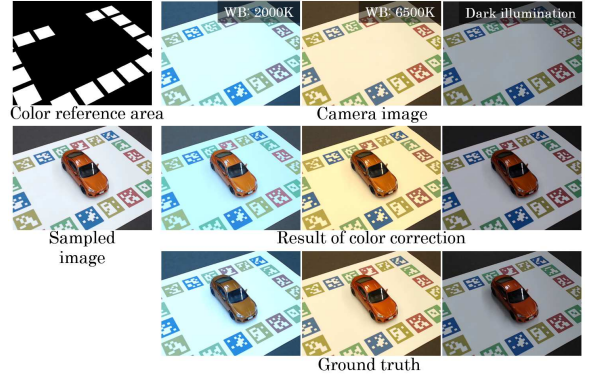


Figure 8: Experimental conditions and the results of color correction: (top-left) color reference area for color correction; (top-right) camera images (used as target color); (middle-left) sampled image (used as source image); (middle-right) results of color correction; (bottom-right) ground truth.

justed to a color temperature of 2000K and 6500K and under a dark illumination environment where some fluorescent lamps were switched off (Fig. 8, bottom-right) are used as ground truth. The images capturing only the marker board by removing the car model under each condition are used for the camera images (Fig. 8, top-right). The color reference area is calculated as shown in the white area of Fig. 8 (top-left). Then, color correction of the sampled image was performed.

The results of color correction are shown in Fig. 8 (middle-right). Comparing the camera images with the results of color correction, it can be clearly seen that their color tone corresponds closely. Furthermore, when the results with the ground truths are compared, we found that the color of the car model is similar because the average color difference in the CIELAB color space between the results and the ground truths of each condition is (WB: 2000K) 11.2813, (WB: 6500K) 10.1238, and (dark illumination) 6.57909. Although we cannot claim that the same color as the ground truth is reproduced because there is a *just noticeable difference* in the CIELAB color space of 2.3 (Sharma and Trussell, 1997), strict color reproduction for user perception is outside the scope of this paper since the generated view of the proposed system is viewed through the display of a mobile device with arbitrary color reproduction characteristics.

## 4.3 Demonstration

In order to verify that the proposed system can display objects photorealistically even with anisotropic reflection or microstructures that make them difficult to render using computer graphics, we implemented

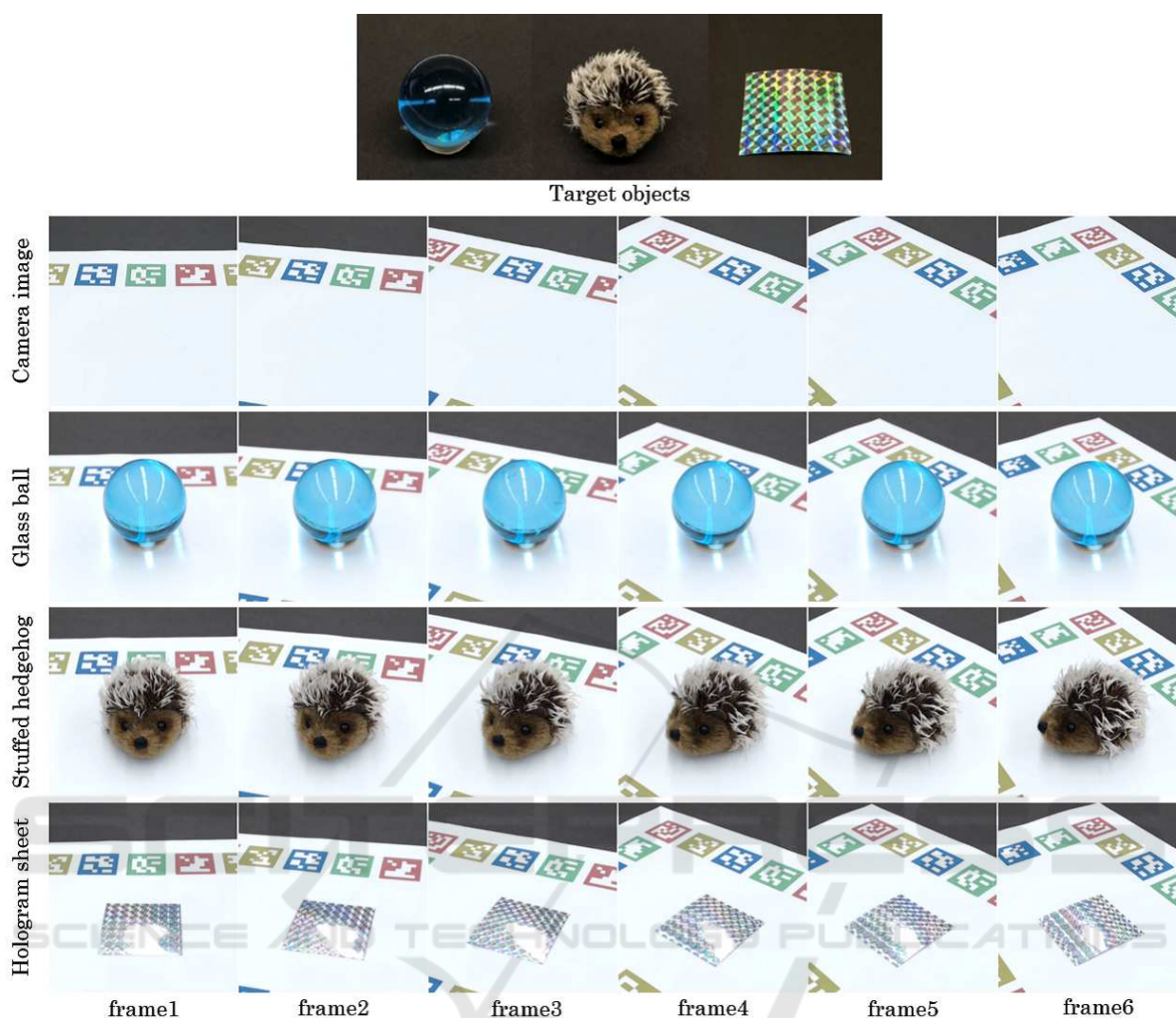


Figure 9: (Top) target objects; (bottom) sequences of the generated views of the proposed system for demonstration.

the prototype system on a PC and conducted a demonstration. Three objects as shown in Fig. 9 (top) are used as targets: glass ball, stuffed hedgehog, and hologram sheet. The target objects were placed on the marker board, and we captured them manually from all angles and stored the pictures as sampled images, using a manual turntable to rotate objects and a tripod to move the camera up and down. In our experimental environment, the number of sampled images was respectively 3741, 3442 and 3665 for each target object.

Fig. 9 (bottom) shows the sequences of the generated views of the proposed system (see supplementary video for the entire sequences). Looking at the generated views of the glass ball and stuffed hedgehog, the condensed light and the distorted background by the glass ball can be seen naturally and the fluffy stuffed hedgehog is faithfully reproduced, but it is difficult to render with computer graphics. Also, looking at the displayed images of the hologram sheet, we can see

how the color of the reflected light of the hologram sheet changes depending on the viewing angle. Since such anisotropic reflection requires considerable time and cost for measurement (Ward et al., 2014), it is difficult to create a 3D model and reproduce it with conventional augmented reality.

#### 4.4 Subjective Experiment

We conducted a subjective experiment to verify whether the proposed system could display real objects more photorealistically than conventional augmented reality. The target object was the car model shown in Fig. 10(b) and 3747 sampled images were captured manually in advance from all angles. The proposed system was implemented on an ASUS smartphone (Zenfone AR: CPU Snapdragon 821, RAM 8 GB). The selected sampled image is read from the storage (UFS 2.0) frame-by-frame and the



Figure 10: Example of the displayed image used in the subjective experiment: (a) Conventional augmented reality; (b) Proposed system.

frame rate was 6-7 fps in this environment with an image size of 1280x720. A conventional augmented reality application was implemented using Vuforia and Unity to render the model of the same car provided by *SQUIR*<sup>3</sup> as shown in Fig. 10(a), employing the shader of *Pro Car Paint Shader*<sup>4</sup> available at Unity Asset Store to present a realistic car model.

In the experiment, 19 participants aged from 25 to 59 years, some of whom had expertise in image processing, were asked to view the display of the proposed system and the conventional augmented reality from various angles in any way they wished, and were then asked to give their impressions of the display by answering a questionnaire. The questions are shown in Fig. 11. Q1 to Q5 are about the naturalness of the displayed image, and Q6 and Q7 ask about the reality and the presence of the target object. The response to each question is evaluated on a 5-grade Likert scale.

The results of the questionnaire evaluation are also shown in Fig. 11. The Wilcoxon signed-rank test was performed and revealed a significant difference ( $p < 0.01$ ) between groups for Q1, Q2, Q3 and Q7. From these results, we can say that the proposed method displays the color, reflection, shadow and shade more naturally than conventional augmented reality. Furthermore, the proposed method can present objects more photorealistically than conventional augmented reality. On the other hand, there is no significant difference between groups for Q4 and Q5 despite the fact that the proposed system displays the object using planar images that have undergone geometric transformation. This result supports the effectiveness of sequential similarity transformation.

Finally, we can find a weakly significant difference ( $p = 0.07$ ) for Q6. This can probably be attributed to the frame rate of the proposed system being considerably lower than conventional augmented reality. While conventional augmented reality renders smoothly at about 30 fps, the proposed system generates a partially jumpy displayed image at 6-7 fps due to processing load and discontinuity of the sampled images. Even though no one commented that

<sup>3</sup><https://squir.com/>

<sup>4</sup><https://www.assetstoresales.com/>

they felt the jumpy displayed image was unnatural, the frame rate and the jumpy displayed image are issues that need to be improved.

## 5 DISCUSSION

There are three major limitations of our system. First, the sampling density and uniformity may crucially affect the quality of generated views, although we confirmed that our system can present satisfactory new views from sampled images created simply using a manual turntable to rotate the objects and a tripod to move the camera up and down. To address this, we can introduce a view interpolation technique derived from image-based rendering, and generate densely and uniformly sampled images on the virtual sphere covering the entire 3D object, employing the method described by Chen and Rosenberg (Chen and Rosenberg, 2018). However, one of the difficult issues of image-based rendering still remains, namely, undesirable artifacts of blurring and edge ghosting. Furthermore, the storage cost depends on the sampling density (660MB in our subjective experiment) and it is better to employ the data compression technique, e.g. the method described by Ishigami et al. (Ishigami et al., 2016), in practical use.

Second, if the visual marker is placed under different lighting conditions, the highlights on the displayed object and shadow/shade will be inconsistent with the real-environment, which is an inherent problem in sampling based methods including image-based rendering, even though the differences of brightness and color tone can be corrected by the method described in Section 3.3. With that in mind, we can provide two examples of application which would not be affected by the above problem.

### Reproduction of Cultural Assets in the Museum

In museums, the lighting environment is usually fixed, and our system can be applied effectively to exhibit cultural assets which are held in the museum's storage facility. It is impossible to exhibit thousands of stored assets because space is limited, but once images of them being exhibited have been captured, they can be viewed as though they were on exhibition at any time.

### Item Browsing in an Electronic Commerce

In this case, the lighting environment at the time of viewing is fundamentally different from the one at the time of capturing. However, users are primarily inter-

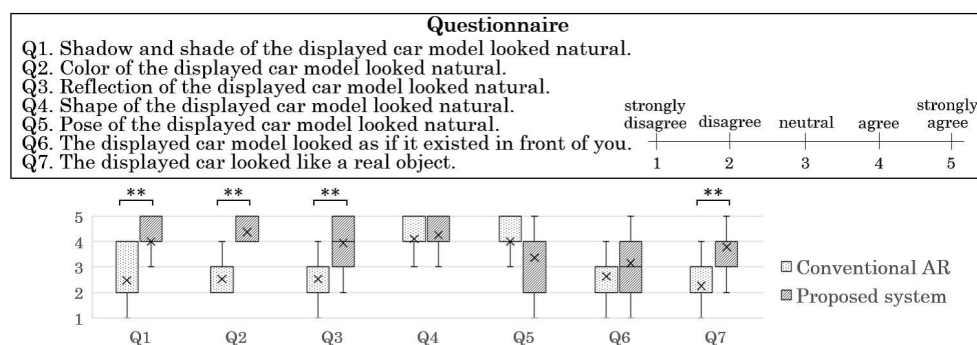


Figure 11: Questionnaire and participant's answers represented as a box plot and the result of statistical analysis of the subjective experiment.

ested in the feel of the item material, and users can view the appearance of the items naturally with our system even if the lighting environment reproduced on the screen is different from the user's environment.

Third, if another object come in the view of the proposed system, the augmented reality experience of the camera, the augmented reality experience of the proposed system may be inhibited because the user is looking at the offline sampled views with only thinking that it is augmented reality. If the region of the interrupting object are extracted from the camera view by the detection and segmentation technique (He et al., 2017), the object can be superimposed in the generated view of the proposed system. However the occlusion culling is still difficult because it needs to estimate the depth information from the single camera view in real time.

## 6 CONCLUSIONS

In this research, we propose a novel system for use on mobile devices capable of reproducing real objects photorealistically from all angles based on new view generation using densely sampled images. In order to realize the proposed system, we developed a method of selecting the image closest to a given camera view from densely sampled images by quantifying the similarity of two rays, performed rigid geometric transformation to preserve the vertical direction for stable viewing, and introduced color correction to maintain the consistency of color between the generated view and the real world. We conducted several experiments to verify the proposed methods and confirmed that these methods worked effectively. Then, we demonstrated that the proposed system can reproduce objects with anisotropic reflection or microstructures using a prototype system. Finally, we conducted a subjective experiment and validated that the proposed system can reproduce objects naturally and photorealistically compared to conventional aug-

mented reality.

In future work, we will attempt to speed up the process using the technique of approximate nearest neighbors search and introduce image interpolation techniques to make the displayed images smoother.

## REFERENCES

- Alcantarilla, P., Nuevo, J., and Bartoli, A. (2013). Fast explicit diffusion for accelerated features in nonlinear scale spaces. In *Proceedings of the British Machine Vision Conference*. BMVA Press.
- Chen, C. and Rosenberg, E. S. (2018). Virtual content creation using dynamic omnidirectional texture synthesis. In *2018 IEEE Conference on Virtual Reality and 3D User Interfaces (VR)*, pages 1–2. IEEE.
- Debevec, P. E., Taylor, C. J., and Malik, J. (1996). Modeling and rendering architecture from photographs: A hybrid geometry-and image-based approach. In *Proceedings of the 23rd annual conference on Computer graphics and interactive techniques*, pages 11–20. ACM.
- Garrido-Jurado, S., Muñoz-Salinas, R., Madrid-Cuevas, F. J., and Marín-Jiménez, M. J. (2014). Automatic generation and detection of highly reliable fiducial markers under occlusion. *Pattern Recognition*, 47(6):2280–2292.
- Gortler, S. J., Grzeszczuk, R., Szeliski, R., and Cohen, M. F. (1996). The lumigraph. In *Proceedings of the 23rd annual conference on Computer graphics and interactive techniques*, pages 43–54. ACM.
- He, K., Gkioxari, G., Dollár, P., and Girshick, R. (2017). Mask r-cnn. In *Computer Vision (ICCV), 2017 IEEE International Conference on*, pages 2980–2988. IEEE.
- Ishigami, F., Nagata, K., Ohta, M., and Yamashita, K. (2016). Data compression for photo-based augmented reality on a tablet. In *Consumer Electronics, 2016 IEEE 5th Global Conference on*, pages 1–2. IEEE.
- Levoy, M. and Hanrahan, P. (1996). Light field rendering. In *Proceedings of the 23rd annual conference on Com-*

- puter graphics and interactive techniques, pages 31–42. ACM.
- Mukaigawa, Y., Sumino, K., and Yagi, Y. (2009). Rapid brdf measurement using an ellipsoidal mirror and a projector. *IPSS Transactions on Computer Vision and Applications*, 1:21–32.
- Nicodemus, F. E., Richmond, J. C., Hsia, J. J., Ginsberg, I. W., and Limperis, T. (1977). *Geometrical considerations and nomenclature for reflectance*, volume 160. US Department of Commerce, National Bureau of Standards.
- Ohta, M., Sato, T., Motokurumada, M., and Yamashita, K. (2013). Real-time color correction for a photo-based augmented reality system. In *Consumer Electronics (GCCE), 2013 IEEE 2nd Global Conference on*, pages 102–103. IEEE.
- Ohta, M., Yokomichi, R., Motokurumada, M., and Yamashita, K. (2012). A photo-based augmented reality system with html5/javascript. In *Consumer Electronics (GCCE), 2012 IEEE 1st Global Conference on*, pages 425–426. IEEE.
- Reinhard, E., Adhikhmin, M., Gooch, B., and Shirley, P. (2001). Color transfer between images. *IEEE Computer graphics and applications*, 21(5):34–41.
- Rock, I. (1974). The effect of retinal and phenomenal orientation of the perception of form. *Scientific American*, 230(1):78–86.
- Rublee, E., Rabaud, V., Konolige, K., and Bradski, G. (2011). Orb: An efficient alternative to sift or surf. In *Computer Vision (ICCV), 2011 IEEE international conference on*, pages 2564–2571. IEEE.
- Ruderman, D. L., Cronin, T. W., and Chiao, C.-C. (1998). Statistics of cone responses to natural images: implications for visual coding. *JOSA A*, 15(8):2036–2045.
- Shade, J., Gortler, S., He, L.-w., and Szeliski, R. (1998). Layered depth images. In *Proceedings of the 25th annual conference on Computer graphics and interactive techniques*, pages 231–242. ACM.
- Sharma, G. and Trussell, H. J. (1997). Digital color imaging. *IEEE Transactions on Image Processing*, 6(7):901–932.
- Shum, H.-Y., Sun, J., Yamazaki, S., Li, Y., and Tang, C.-K. (2004). Pop-up light field: An interactive image-based modeling and rendering system. *ACM Transactions on Graphics (TOG)*, 23(2):143–162.
- Sinha, S. N., Kopf, J., Goesele, M., Scharstein, D., and Szeliski, R. (2012). Image-based rendering for scenes with reflections. *ACM Trans. Graph.*, 31(4):100–1.
- Suzuki, K., Wakisaka, S., and Fujii, N. (2012). Substitutional reality system: a novel experimental platform for experiencing alternative reality. *Scientific reports*, 2:srep00459.
- Tsai, R. (1987). A versatile camera calibration technique for high-accuracy 3d machine vision metrology using off-the-shelf tv cameras and lenses. *IEEE Journal on Robotics and Automation*, 3(4):323–344.
- Tunwattanapong, B., Fyffe, G., Graham, P., Busch, J., Yu, X., Ghosh, A., and Debevec, P. (2013). Acquiring reflectance and shape from continuous spherical harmonic illumination. *ACM Transactions on graphics (TOG)*, 32(4):109.
- Vaghvarshakyan, S., Bregovic, R., and Gotchev, A. (2015). Image based rendering technique via sparse representation in shearlet domain. In *2015 IEEE International Conference on Image Processing (ICIP)*, pages 1379–1383. IEEE.
- Ward, G., Kurt, M., and Bonneel, N. (2014). Reducing anisotropic bsdf measurement to common practice. In *Material Appearance Modeling*, pages 5–8.
- Wood, D. N., Azuma, D. I., Aldinger, K., Curless, B., Duchamp, T., Salesin, D. H., and Stuetzle, W. (2000). Surface light fields for 3d photography. In *Proceedings of the 27th annual conference on Computer graphics and interactive techniques*, pages 287–296. ACM Press/Addison-Wesley Publishing Co.